



Evidence of multiple nodeless energy gaps in superconducting $\text{Ba}_{0.6}\text{K}_{0.4}\text{Fe}_2\text{As}_2$ single crystals from scanning tunneling spectroscopy

Lei Shan,^{1,*} Yong-Lei Wang,¹ Jing Gong,¹ Bing Shen,¹ Yan Huang,¹ Huan Yang,¹ Cong Ren,¹ and Hai-Hu Wen^{1,2,†}

¹National Laboratory for Superconductivity, Institute of Physics & Beijing National Laboratory for Condensed Matter Physics, Chinese Academy of Sciences, P.O. Box 603, Beijing 100190, China

²National Laboratory of Solid State Microstructures and Department of Physics, Nanjing University, Nanjing 210093, China

(Received 27 August 2010; revised manuscript received 4 January 2011; published 28 February 2011)

We report on low-temperature scanning tunneling microscopy and spectroscopy (STM) studies of the electronic structure of single-crystalline $\text{Ba}_{0.6}\text{K}_{0.4}\text{Fe}_2\text{As}_2$. Multiple superconducting gaps are observed in the density of states (DOS) and the sizes of the two dominant gaps Δ_L and Δ_S are 7.6 and 3.3 meV, respectively. The flat bottom of the DOS spectra near zero bias indicates the nodeless feature of the gaps, while the global fitting to the spectra definitely requires the anisotropy. The nodeless gaps with finite anisotropy revealed in our STM data agree well with the expectations of an extended *s*-wave superconductivity.

DOI: [10.1103/PhysRevB.83.060510](https://doi.org/10.1103/PhysRevB.83.060510)

PACS number(s): 74.70.Xa, 74.55.+v, 74.20.Rp

A new family of high-temperature superconductors, iron pnictides,^{1–6} have attracted extensive attention in recent years. It has been proposed theoretically that their superconductivity is mediated by antiferromagnetic spin fluctuations, which induces a singlet superconducting order parameter with a sign reversal between different Fermi-surface sheets, known as the S_{\pm} pairing form.^{7–13} Depending on the details of the band structure, the S_{\pm} form factor can evolve to a nodal S_{\pm} form factor. In other words, the nodal structure in the superconducting gap is not requested by the symmetry in these multiband superconductors, which is in contrast to the case of cuprates.¹⁴ To verify this model, it is particularly important to investigate the superconducting gaps of various Fermi-surface sheets, which can be measured directly in real space and momentum space by scanning tunneling microscopy and spectroscopy (STM) and angle-resolved photoemission spectroscopy (ARPES), respectively. Recently, an S_{\pm} pairing with a full gap was demonstrated by STM studies in an iron chalcogenide Fe(Se, Te).¹⁵ Such an isotropic gap is qualitatively consistent with that obtained in another STM experiment¹⁶ and with ARPES data,¹⁷ although the exact gap sizes are quite different. For iron pnictides, however, the current results have not yet been reconciled. ARPES data almost always present multiple gaps with weak anisotropy.^{18–25} However, due to the unsatisfactory energy resolution of ARPES, the reported gap magnitudes are far from agreement and it cannot be distinguished whether there are some tiny nodal regions (or accidental nodes) in the superconducting gap functions. Therefore, STM experiments on the same samples are strongly desirable since they have much better energy resolution. Unfortunately, all the previous STM data give a single gap (except a most recent report²⁶) and its anisotropy (nodal or nodeless) cannot be definitely determined due to the finite zero-bias conductance in the measured spectra.^{21,26–29} This may be due to the inadequate surface quality of the studied samples or some intrinsic origins such as the scattering effect of the dopants in the superconducting FeAs layer in some samples. In order to clarify this issue, further experimental evidence is desirable.

In this paper, we present experimental evidence from STM measurements for the multiband superconductivity in

iron-pnictide superconductors. On the measured spectra of differential conductance versus sample bias voltage, multiple gaps are observed. The zero density of states (DOS) in a finite energy scope around zero bias excludes the existence of nodes in the gaps.

The nearly optimally doped $\text{Ba}_{0.6}\text{K}_{0.4}\text{Fe}_2\text{As}_2$ ($T_c = 37$ K) single crystals studied here were grown with self-flux method.³⁰ As shown in Fig. 1(a), the onset temperature of the superconducting transition is 37.2 K with a transition width of 1.8 K (determined from the peak width in the imaginary part of the ac susceptibility). In the STM experiments, the single-crystalline sample is cold-cleaved *in situ*, then immediately inserted into the microscope, which is already at the desired temperature. All the STM data presented here were recorded at 3 K.

Figure 1(b) shows a typical topographic image often obtained. The surface is flat with an rms deviation below 1 Å, which is similar to the cleavage reported previously.²¹ A small region is magnified in Fig. 2(a); it can be seen clearly that the surface is spread with disordered bright “clusters” with diameters of from ~ 5 Å to ~ 15 Å. Since FeAs layers usually exhibit a well-ordered atomic lattice,^{29,31–34} the highly disordered surface observed here is most likely to be the (Ba, K) layer.

In order to investigate the superconducting gaps of $\text{Ba}_{0.6}\text{K}_{0.4}\text{Fe}_2\text{As}_2$, spatially resolved tunneling spectroscopy measurements were carried out on the sample surfaces. We have recorded differential conductance dI/dV versus sample-tip bias voltage V in a dense array of locations covering the region shown in Fig. 2(a). Since dI/dV is proportional to the local DOS and V corresponds to the energy of quasiparticles, we can extract the magnitude of the superconducting gap by measuring the distance between coherence peaks in the spectra of dI/dV versus V . It was found that all the measured spectra show clear superconducting gaps characterized by prominent coherence peaks and remarkable DOS suppression between them. Actually, almost all curves have a flat bottom at low energies with zero density of states [refer to Figs. 3(b) and 4]. Moreover, the majority of the curves reveal a two-gap structure, where the smaller gap is estimated to be $2 \sim 4.5$ meV and the larger gap is $6.5 \sim 9$ meV. In comparison with the data

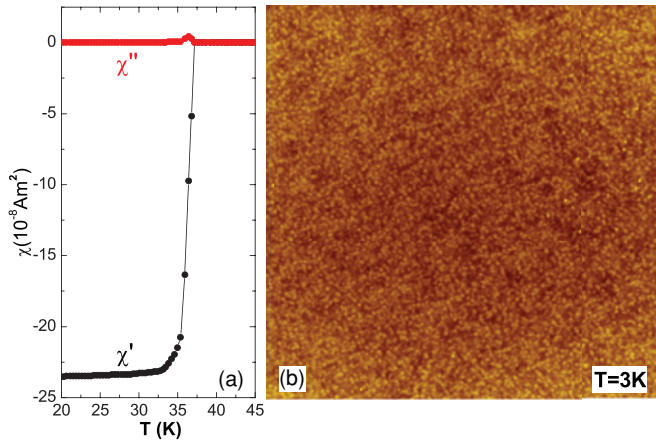


FIG. 1. (Color online) (a) Temperature dependence of the ac susceptibility of a $\text{Ba}_{0.6}\text{K}_{0.4}\text{Fe}_2\text{As}_2$ single crystal used in this work. The measurements were performed with an Oxford Maglab-Exa-12 system with an ac field of 0.1 Oe and an oscillation frequency of 133 Hz. The half-height width of the imaginary component is about 1 K. (b) 133 nm \times 133 nm topographic STM image of the $\text{Ba}_{0.6}\text{K}_{0.4}\text{Fe}_2\text{As}_2$ single crystal cold-cleaved *in situ*. It was taken with a sample-tip voltage of 50 mV and tunneling current of 200 pA.

obtained on another type of cleaved surface,³⁵ we found that the surface configuration indeed affects the spectral shape (such as inducing finite low-bias conductance in some cases), while it does not completely conceal the two-gap feature and change the gap values significantly.

To exemplify the observations mentioned above, Fig. 2(b) shows the spectra recorded along the white line denoted in Fig. 2(a). The vertical lines indicate the features of both the smaller gap (Δ_S) and the larger one (Δ_L). Although the coherence peaks of Δ_L are obvious on almost all curves, the Δ_S peaks become prominent only on some of the curves and they behave more like “knees” on the other curves. This indicates that the measured spectral weight contributed by different bands varies from one position to another on the sample surface, which is not understood at the present time. Nonetheless, the superconducting gaps are homogeneous on a much larger scale. Figures 2(c) and 2(d) show the maps of the gaps below and above 6 meV, respectively, reflecting the spatial distribution of Δ_S and Δ_L . The black areas in the figures indicate that there is no prominent gap feature in the selected energy range. It was found that the larger gap and the smaller one can be detected simultaneously almost everywhere on the sample surface. Moreover, the gap values can be homogeneous over the quite large scale from 20 Å to beyond 100 Å. It was noted that, at some local regions (in a scale below 2 nm), the spectra are strongly asymmetric at low biases in addition to the overall inclined background [for example, see curves 2, 3 and 15, 16 at the bottom in Fig. 2(b)]. Such regions possess below 10 percent of the investigated area shown in Fig. 2. According to our preliminary data taken at higher temperatures, this is possibly related to a local state with a conductance peak (or hump) at a finite positive bias, which may contribute an asymmetric spectral shape. However, up to now, we cannot say that the local state is a surface state due to the random distribution of surface atoms or that it is determined by the lower layers of the sample (such as

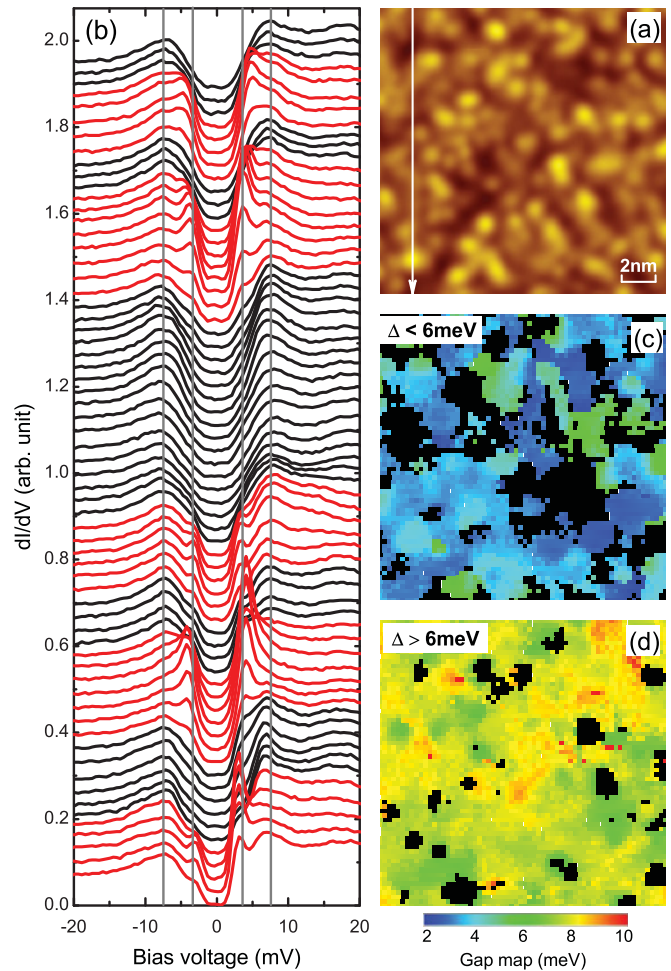


FIG. 2. (Color online) (a) Zoom in on a 17 nm \times 17 nm area within Fig. 1(b), which is taken at 3 K. (b) Spatially resolved spectra of dI/dV versus V recorded along the trajectory (white line) indicated in (a) with a spacing interval of 2.7 Å. The four vertical lines are to guide the eye. (c), (d) Maps of the superconducting gap determined in the energy ranges below and above 6 meV, respectively.

impurities in the single crystal). This issue indeed deserves further investigation. Here, we call the majority of the curves without the strong low-bias asymmetry “typical curves.”

Figure 3(a) shows the histogram of the obtained gap magnitude, in which two peaks are located at about 3 and 8 meV. By fitting the data to a multipole Gaussian function, we obtained the two values $\Delta_S = 3.3$ meV and $\Delta_L = 7.6$ meV. It was noted that the coherence peaks contributed from Δ_L are broader than that expected by a single gap. To get further insight into this issue, we have examined the spectra where Δ_L is dominant in spectral weight. On these curves, as shown in Fig. 3(b), another peak or shoulder outside the coherence peak of Δ_L can be distinguished. This feature has an energy scale of around 10 meV and most likely indicates another superconducting gap. Because this gap is very close to Δ_L in magnitude and its contribution looks much weaker than that from the other two gaps, it is difficult to identify in our statistical analysis presented in Fig. 3(a). Multiple gaps of 3.3, 7.6, and ~ 10 meV correspond to the gap ratio $2\Delta/(k_B T_c)$ of about 2.1, 4.8, and 6.3, respectively, which are

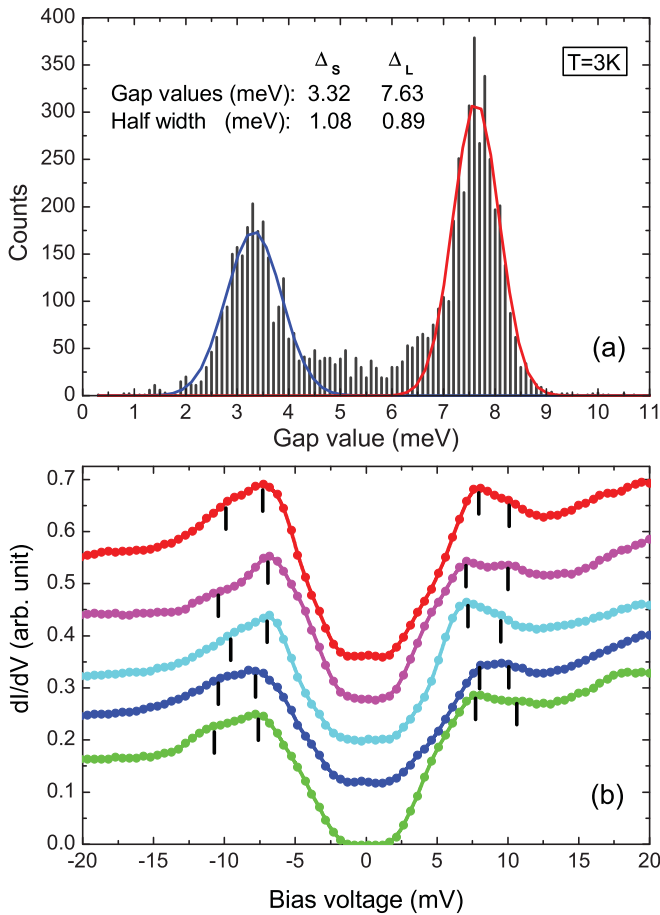


FIG. 3. (Color online) (a) Histogram of the obtained superconducting gaps. The fit to a multipeak Gaussian function is also plotted here with a list of the fitting parameters. (b) Some spectra measured at different locations on the sample surface. Both coherence peaks of Δ_L and the features of a larger gap (broad peaks or humps) are indicated by short black bars. A slight kink feature contributed from Δ_S can still be distinguished, although for clarity it is not marked here.

much smaller or much larger than the value of 3.53 expected by weak-coupling BCS theory. The gaps observed here are qualitatively consistent with our previous penetration-depth measurements, which give $\Delta_L^{\text{pen}} = 9$ meV and $\Delta_S^{\text{pen}} = 2.5$ meV.³⁶ Most notably, the gap magnitudes determined here are in good agreement with the recent results derived from specific heat data, which give gap values of 3.6, 8.5, and 9.2 meV.³⁷ Furthermore, the most recent ARPES experiment²⁴ detected the gaps of 12, 7, and 4 meV on the hole-like Fermi surfaces, and a 9.5-meV gap on the electron-like Fermi surfaces. The relative size of the gaps revealed by ARPES are similar to that observed here by STM, in spite of the difference of the absolute values, indicating the qualitative consistency between the measurements of momentum space and real space.

In order to get a more quantitative understanding of the superconducting gaps, some typical spectra measured at different locations are normalized by a slope background, as shown in Fig. 4. It can be seen that the bottom of these curves are flat to zero, giving strong evidence that the gaps observed here are nodeless. The coherence peaks of Δ_S are

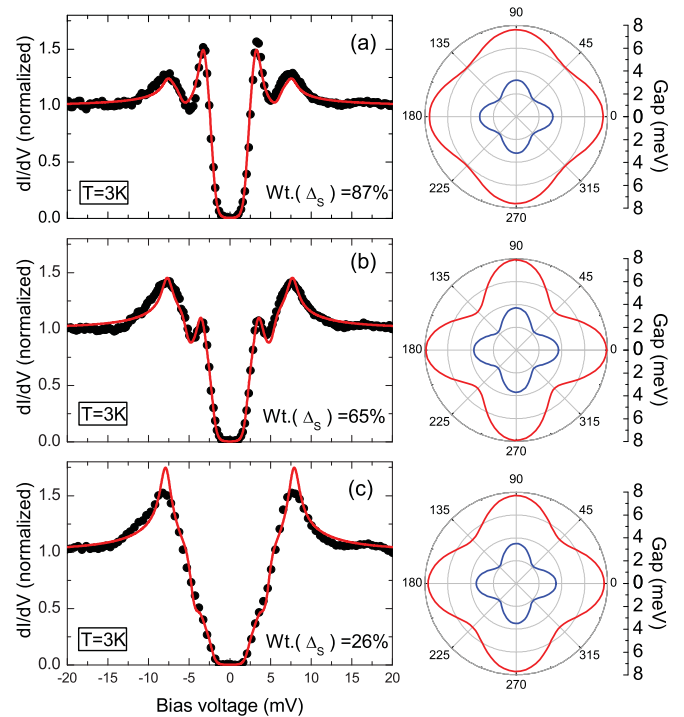


FIG. 4. (Color online) Left column: Typical spectra measured at different positions on the sample surface (black dots). The curves are the fits to the two-band model discussed in the text. $\text{Wt.}(\Delta_S)$ means the spectral weight contributed from Δ_S , which is equal to the parameter σ mentioned in the text. Right column: Gap functions for the two gaps assumed in the fitting. It was noted that the adaptive gaps in these simulations should be nodeless and have a small anisotropy. The calculated coherence peaks for the larger gap (Δ_L) look more narrow than the experimental data, which may be due to the neglect of the contribution from the ~ 10 meV gap, as illustrated in Fig. 3(b).

weakened from (a) to (c), indicating the variation of the contributions from different bands, as mentioned above. Since the spectral weight of the ~ 10 -meV gap is very weak, we take a simple two-band model to simulate the data. The formula was constructed as follows: $G_{SN} = \sigma dI_{SN}^S/dV + (1 - \sigma)dI_{SN}^L/dV$ (σ is the spectral weight contributed from one of the two bands), where $I_{SN}^{S(L)} \propto \int_{-\infty}^{\infty} d\varepsilon \int_0^{2\pi} d\theta [f(\varepsilon) - f(\varepsilon + eV)] \text{Re}(|\varepsilon + eV| [(\varepsilon + eV)^2 - \Delta_{S(L)}^2(\theta)]^{-1/2})$ are the expressions for the tunneling current, and the superscripts S and L correspond to $\Delta_S(\theta)$ and $\Delta_L(\theta)$, respectively. Here, we take the anisotropic gap functions $\Delta_{S(L)}(\theta) = \Delta_{S(L)}^0 [x \cos(4\theta) + 1 - x]$ for both gaps, in which x determines the gap anisotropy. It should be pointed out that this particular function is selected just for taking into account the possible anisotropy and should not be exclusive.

As shown in Fig. 4, the two-band model fits the main features very well for all the data. The exact gap functions used in fitting are shown in the right column of the figure. Although the spectra were recorded at different positions, the gap functions determined by fitting are close to each other; namely, they have similar gap magnitudes of $\Delta_L^0 = 7.7 \pm 0.2$ meV and $\Delta_S^0 = 3.5 \pm 0.2$ meV with the anisotropy below 3.2 and 1.5 meV, respectively. The only significant difference between them is the spectral weight of Δ_S (Δ_L), which varies from

87% (13%) to 26% (74%). According to the data obtained on $\text{Ba}_{0.6}\text{K}_{0.4}\text{Fe}_2\text{As}_2$, it could be concluded that the nodal structure of the superconducting gaps is accidental and not requested by the symmetry in the iron-pnictide superconductors, which is consistent with the previous theoretical predictions.⁷⁻¹³

To summarize, we have studied low-temperature scanning tunneling microscopy and spectroscopy on the hole-doped iron-pnictide superconductor $\text{Ba}_{0.6}\text{K}_{0.4}\text{Fe}_2\text{As}_2$. The measured spectra of differential conductance versus sample-tip voltage exhibit clear multigap features. The magnitudes of the gaps were estimated to be 3.3, 7.6, and ~ 10 meV. The bottom of

the spectra is flat to zero in a finite-energy window, excluding the existence of nodes in the gaps. The multiple nodeless superconducting gaps observed here provide strong evidence of S_{\pm} pairing in iron-pnictide superconductors.

The authors are grateful for kind help from Dr. Ang Li and Prof. Shuheng Pan during the STM measurements. This work is supported by the Natural Science Foundation of China, the Ministry of Science and Technology of China (973 project No: 2011CBA00100, 2010CB923002), and the Chinese Academy of Sciences.

*lshan@aphy.iphy.ac.cn

†hhwen@aphy.iphy.ac.cn

¹Y. Kamihara, T. Watanabe, M. Hirano, and H. Hosono, *J. Am. Chem. Soc.* **130**, 3296 (2008).

²X. H. Chen, T. Wu, G. Wu, R. H. Liu, H. Chen, and D. F. Fang, *Nature (London)* **453**, 761 (2008).

³H.-H. Wen, G. Mu, L. Fang, H. Yang, and X. Zhu, *Europhys. Lett.* **82**, 17009 (2008).

⁴G. F. Chen, Z. Li, D. Wu, G. Li, W. Z. Hu, J. Dong, P. Zheng, J. L. Luo, and N. L. Wang, *Phys. Rev. Lett.* **100**, 247002 (2008).

⁵Z.-A. Ren *et al.*, *Chin. Phys. Lett.* **25**, 2215 (2008).

⁶M. Rotter, M. Tegel, and D. Johrendt, *Phys. Rev. Lett.* **101**, 107006 (2008).

⁷I. I. Mazin, D. J. Singh, M. D. Johannes, and M. H. Du, *Phys. Rev. Lett.* **101**, 057003 (2008).

⁸K. Kuroki, S. Onari, R. Arita, H. Usui, Y. Tanaka, H. Kontani, and H. Aoki, *Phys. Rev. Lett.* **101**, 087004 (2008).

⁹Z.-J. Yao, J.-X. Li, and Z. D. Wang, *New J. Phys.* **11**, 025009 (2009).

¹⁰K. Seo, B. A. Bernevig, and J. Hu, *Phys. Rev. Lett.* **101**, 206404 (2008).

¹¹F. Wang, H. Zhai, Y. Ran, A. Vishwanath, and D.-H. Lee, *Phys. Rev. Lett.* **102**, 047005 (2009).

¹²A. V. Chubukov, D. V. Efremov, and I. Eremin, *Phys. Rev. B* **78**, 134512 (2008).

¹³W.-Q. Chen, K.-Y. Yang, Y. Zhou, and F.-C. Zhang, *Phys. Rev. Lett.* **102**, 047006 (2009).

¹⁴M. R. Norman and C. Pépin, *Rep. Prog. Phys.* **66**, 1547 (2003).

¹⁵T. Hanaguri, S. Niitaka, K. Kuroki, and H. Takagi, *Science* **328**, 474 (2010).

¹⁶T. Kato, Y. Mizuguchi, H. Nakamura, T. Machida, H. Sakata, and Y. Takano, *Phys. Rev. B* **80**, 180507 (2009).

¹⁷K. Nakayama *et al.*, *Phys. Rev. Lett.* **105**, 197001 (2010).

¹⁸H. Ding, P. Richard *et al.*, *EPL* **83**, 47001 (2008).

¹⁹L. Zhao *et al.*, *Chin. Phys. Lett.* **25**, 4402 (2008).

²⁰T. Kondo *et al.*, *Phys. Rev. Lett.* **101**, 147003 (2008).

²¹L. Wray *et al.*, *Phys. Rev. B* **78**, 184508 (2008).

²²D. V. Evtushinsky *et al.*, *Phys. Rev. B* **79**, 054517 (2009).

²³K. Nakayama *et al.*, *Europhys. Lett.* **85**, 67002 (2009).

²⁴Y. Zhang *et al.*, *Phys. Rev. Lett.* **105**, 117003 (2010).

²⁵Y.-M. Xu *et al.*, e-print arXiv:1006.3958.

²⁶M. L. Teague, G. K. Drayna, G. P. Lockhart, P. Cheng, B. Shen, H.-H. Wen, and N.-C. Yeh, e-print arXiv:1007.5086.

²⁷M. C. Boyer, K. Chatterjee, W. D. Wise, G. F. Chen, J. L. Luo, N. L. Wang, and E. W. Hudson, e-print arXiv:0806.4400.

²⁸O. Millo, I. Asulin, O. Yuli, I. Felner, Z.-A. Ren, X.-L. Shen, G.-C. Che, and Z.-X. Zhao, *Phys. Rev. B* **78**, 092505 (2008).

²⁹Y. Yin, M. Zech, T. L. Williams, X. F. Wang, G. Wu, X. H. Chen, and J. E. Hoffman, *Phys. Rev. Lett.* **102**, 097002 (2009).

³⁰H. Luo, Z. Wang, H. Yang, P. Cheng, X. Zhu, and H.-H. Wen, *Supercond. Sci. Technol.* **21**, 125014 (2008).

³¹V. B. Nascimento, A. Li *et al.*, *Phys. Rev. Lett.* **103**, 076104 (2009).

³²F. C. Niestemski, V. B. Nascimento, B. Hu, W. Plummer, J. Gillett, S. Sebastian, Z. Wang, and V. Madhavan, e-print arXiv:0906.2761.

³³F. Masee, S. de Jong, Y. Huang, J. Kaas, E. van Heumen, J. B. Goedkoop, and M. S. Golden, *Phys. Rev. B* **80**, 140507 (2009).

³⁴T.-M. Chuang, M. P. Allan, J. Lee, Y. Xie, N. Ni, S. L. Bud'ko, G. S. Boebinger, P. C. Canfield, and J. C. Davis, *Science* **327**, 181 (2010).

³⁵L. Shan *et al.*, *Nature Physics* (2011), doi:10.1038/nphys1908.

³⁶C. Ren, Z.-S. Wang, H.-Q. Luo, H. Yang, L. Shan, and H.-H. Wen, *Phys. Rev. Lett.* **101**, 257006 (2008).

³⁷P. Popovich, A. V. Boris, O. V. Dolgov, A. A. Golubov, D. L. Sun, C. T. Lin, R. K. Kremer, and B. Keimer, *Phys. Rev. Lett.* **105**, 027003 (2010).